Indian Journal of Pure & Applied Physics
Vol. 56, October 2018, pp. 773-786

Chemically reacting and radiating nanofluid flow past an exponentially stretching sheet in a porous medium

M K Nayak[a]*, Sachin Shaw[b] & O D Makinde[c]

[a] Department of Physics, Radhakrishna Institute of Technology and Engineering, Biju Patnaik University of Technology, Khurda 752 057, India

[b]Department of Mathematics and Computational Sciences, Botswana International University of Science and Technology, Private Bag 16, Palapye, Botswana

[c]Faculty of Military Science, Stellenbosch University, Private Bag X2, Saldanha 7395, South Africa

Received 14 September 2017; accepted 5 April 2018

The influence of non-uniform permeability, thermal radiation and variable chemical reaction on three-dimensional flow of an incompressible nanofluid over an exponentially-stretching sheet in association with a convective boundary condition has been investgated. In the present study, a new micro-convection model known as Patel model has been employed to enhance the thermal conductivity and hence the heat transfer capability of nanofluids. In the present analysis, base fluids such as water, 30% ethylene glycol, 50% ethylene glycol and nanoparticles such as Cu, Ag and Fe_3O_4 have been considered. With the help of some suitable transformations the governing partial differential equationsare converted into a set of ordinary differential equations which have beeen then solved numerically by using fourth-order Runge-Kutta method along with shooting technique. The influence of various embedded physical parameters have been explored through graphs for velocity, temperature, concentration, skin friction, local Nusselt and Sherwood numbers. The resistive force offered by the porous matrix belittles the momentum boundary layer and helps in growing the temperature and concentration boundary layers. Fluid temperature is an increasing function of radiation parameter Rd and Biot's number Bi whereas concentration field is a decreasing function of Schmidt number Sc and chemical reaction parameter γ.

Keywords: Non-uniform porous medium, 3D flow, Convective boundary condition, Thermal Radiation, Variable chemical reaction

1 Introduction

The investigations that remained at the beginning of the 21st century were largely concerned with the development of the boundary layer flow of viscous/viscoelastic fluids over stretching surface and with late investigations of MHD flow over stretching sheet. The beginning of the investigation of the boundary layer flow over stretching surface was made by Sakiadis[1]. Over the years, many noteworthy researchers viz. Crane[2], Khan and Sanjayanand[3], Hayat *et al.*[4] and Makinde *et al.*[5] contributed a lot of endeavors and finally succeeded in the investigation of the boundary layer MHD flow over stretching surfaces. Although their investigations contributed to better cooling due to controlled momentum and heat transfer under the influence of MHD flow, however, they were restricted to lower heat transfer capability and hence could not meet the modern cooling requirements in industrial fields and manufacturing processes. To get rid of such constraints, Choi[6] was the first who pioneered experimentally a significant enhancement in thermal conductivity and hence heat transfer performance through the addition of small amount of nanoparticles viz. metals, oxides, carbides, nitrides and carbon nanotubes (particles of 100 nm or less size) in base fluids such as water, kerosene, engine oil, touline, ethylene glycol and tri-ethylene glycol, etc. (nanofluids). About this time, the phenomenon of thermal conductivity enhancement through the mechanism of suitable dispersion and sustainable suspension of the nanoparticles in the base fluids was maneuvered and significantly observed by many researchers viz. Xuan and Li[7], Khan and Pop[8], Nayak[9] and Akber *et al.*[10]

Because of unexpected thermal properties (higher thermal conductivity) of nanofluids, these are served as best suitable coolants in the numerous applications. Such applications include next generation coolants for computers and safe coolants for nuclear reactors. Further major applications of nanofluids as coolants are in cancer therapy, safer surgery, heat exchangers, micro-channel heat sinks and several electronic devices for use in military sectors, vehicles and transformers, in designing the waste heat removal

*Corresponding author (E-mail: mkn2122@gmail.com)

equipment, major manufacturing industries associated with materials and chemicals, oil and gas, food and drink, paper and printing, polymer extrusion, glass blowing, rapid spray cooling, cooling of microelectronics, wire drawing and quenching in metal foundries and as refrigerant/lubricant mixtures enabling to chill or cool buildings. Nanofluids along with biotechnological components bring forth many potential applications in biological sensors, pharmaceuticals and agriculture. In view of above relevance, many researchers[11-14] have been motivated and encouraged to investigate several aspects of flow and heat transfer of nanofluids over various types of surfaces.

It has to be accepted that porous medium has vital role in the heat transfer advancement in industrial systems that include the application of metal-based porous materials such as copper foams in channels and heat exchangers. Porous medium is a solid matrix that contains pores (voids) which are connected and filled with the fluid completely so that the fluid can flow through the voids. By introducing porous medium, the contact surface area between liquid and solid surface increases and as a consequence, they can be used as insulators and heat transfer promoters in different systems. Furthermore, nanoparticles dispersed in nanofluid enhance the effective thermal conductivity. For these reasons, use of both porous media and nanofluid can enhance the thermal efficiency of typical physical systems significantly. In view of above advantages, porous media finds important applications in oil production, electronic cooling systems, heat exchangers etc. By dint of above relevance, many researchers[15-17] have paid their attention to extensive investigations in this field. In an article, Malik and Nayak[18] investigated numerically (through finite volume simulation) the heat transfer and entropy generation of MHD nanofluid flow in a porous medium where the flow is governed by time periodic discrete heat sources subject to the short side walls in the enclosure. In their study, they accomplished that higher heat transfer is on the cost of least entropy generation and the heat transfer irreversibility is found to be dominant over magnetic field. Since then, in another article, Hobold and Silva[19] addressed in their study that optimal 2D porosity distributions create obstacles in the core flow converging the heated spots near the wall. They also noticed that minimization of wall temperature correlates with enhanced flow velocity subject to heat dissipation. Govender[20] used Darcy model and investigated analytically the thermal instability in a horizontal porous layer filled completely by nanofluid subject to vertical vibration. In the recent past, Roy *et al.*[21] analyzed the heat line visualization in mixed convection inside porous triangular cavities.

It is a known fact that convective boundary condition represents the heat transfer rate through the surface is proportional to the local difference in temperature subject to ambient conditions. In other words, convective boundary condition enhances the temperature and therefore the thermal conductivity of the nanofluids. This is why it is necessary to trumpet the fact that the introduction of the convective boundary condition is more suitable as a model compared to isothermal conditions. Makinde and Aziz[22] implemented the convective boundary condition in a stretched boundary-layer flow of a nanofluid wherein they addressed the larger convection at the surface produces greater penetration of thermal effect in the flow domain. Mustafa and Khan[23] considered slip effects in MHD flow of nanofluid in a stretched rotating disk wherein they observed that steady state rotation of the disk requires minimum rotation subject to Fe_3O_4 nanoparticles.

It is obvious by the fact that thermal radiation effect is important in case of large temperature difference between the boundary surface and ambient fluid. Apart from that it is inevitable for space applications where some devices are developed to operate at high temperature levels so as to accomplish high thermal efficiency. It is due to this reason that radiation effects are significant while determining thermal effects in the processes involving high temperatures such as in the design of many advanced conversion systems. Makinde and Ogulu[24] found by investigation, that increase in thermal radiation enhances the non-dimensional temperature profiles in a flow of a variable viscosity fluid over a vertical porous plate in presence of transverse magnetic field. Nayak[25] analyzed in his study that thermal radiation should be kept minimum so as to achieve more cooling due to MHD viscoelastic fluid flow over a stretching sheet. Further, the researchers[26-32] have paid their efforts in exploration of the thermal radiation effects over different surfaces.

Recent investigations indicate that industrial fluids may be chemically reactive and chemical reaction may alter diffusion rates. As a consequence, diffusion of species involving chemical reaction in boundary

layer flow finds huge applications in the areas include pollution studies, oxidation and synthesis materials and fibrous insulation. Chemical reaction is also considered to be important due to its vital role in the design of chemical processing equipments, processing of food, cooling towers, formation and dispersion of fog, fibrous insulation, moisture and temperature distributions over agricultural fields, damage of crops due to freezing, etc. In view of above significant applications, many authors have investigated and produced their results on chemical reaction effects on the flow of heat and/or mass transfer over different surfaces. Mabood *et al.*[33] discussed the effect of chemical reaction in MHD stagnation point flow under the influence of viscous dissipation. In their study, they observed that increase in chemical reaction rate decreases nanoparticle concentration and show the reverse effect with the rate of mass transfer. The influence of chemical reaction and activation energy associated with buoyancy in magneto-nanofluid flowing over a stretched vertical surface is explored by Mustafa *et al.*[34]. Nanoparticle concentration becomes more with more activation energy of chemical reaction is recorded in their investigation. Many others[35,36] investigated in the related areas with different configurations.

The above literature survey ensures that no one has discussed yet the impact of non-uniform permeability, thermal radiation and variable chemical reaction on three-dimensional nanofluid flow past an exponentially-stretching sheet with a convective boundary condition employing Patel model[37]. Hence, the novelty of our present study is to investigate the influence of non-uniform permeability, thermal radiation and variable chemical reaction in 3D stretched flow of nanofluid staking into account convective boundary conditions. One of the important aspects of the present study deals with the introduction of the Patel model which has the significant role to upsurge the thermal conductivity and hence the heat transfer capability of nanofluids thereby indicating more cooling. In the present analysis, the solution of derived similarity transformed governing boundary layer equations is carried out numerically using the fourth-order Runge-Kutta method along with the shooting technique. The influence of various embedded pertinent physical parameters on the dimensionless velocity, temperature and nanoparticle concentration along with the skin friction, the local Nusselt and Sherwood numbers are well discussed and presented in the form of literature, graphs and tables.

2 Formulation of Problem

We consider a steady three dimensional boundary layer flow of radiating nanofluid over an exponential stretching sheet as shown in Fig. 1. The present analysis is carried out by taking the following assumptions (i) the flow is steady, laminar and incompressible, (ii) the thermal conductivity and specific heat are temperature independent, (iii) gravitational effect is negligible, (iv) convective boundary condition representing heat transfer rate through the surface is introduced and (v) porous media permeability $K = K_0 e^{-\frac{x+y}{2L}}$ is introduced (vi) variable chemical reaction rate $\Omega = \Omega_0 e^{\frac{x+y}{L}}$ is introduced in the flow.

Considering the aforementioned assumptions, the steady boundary layer governing equations indicating conservation of mass, momentum, energy and nanoparticle concentration are:

$$\frac{\partial u}{\partial x}+\frac{\partial v}{\partial y}+\frac{\partial w}{\partial z}=0 \qquad \ldots (1)$$

$$u\frac{\partial u}{\partial x}+v\frac{\partial u}{\partial y}+w\frac{\partial u}{\partial z}=\frac{\mu_{nf}}{\rho_{nf}}\frac{\partial^2 u}{\partial z^2}-\frac{\mu_{nf}u}{\rho_{nf}K} \qquad \ldots (2)$$

$$u\frac{\partial v}{\partial x}+v\frac{\partial v}{\partial y}+w\frac{\partial v}{\partial z}=\frac{\mu_{nf}}{\rho_{nf}}\frac{\partial^2 v}{\partial z^2}-\frac{\mu_{nf}v}{\rho_{nf}K} \qquad \ldots (3)$$

$$u\frac{\partial T}{\partial x}+v\frac{\partial T}{\partial y}+w\frac{\partial T}{\partial z}=\frac{k_{nf}}{(\rho C_P)_{nf}}\frac{\partial^2 T}{\partial z^2}+\frac{16\sigma^* T_\infty^3}{3k^*(\rho C_P)_{nf}}\frac{\partial^2 T}{\partial z^2} \qquad \ldots (4)$$

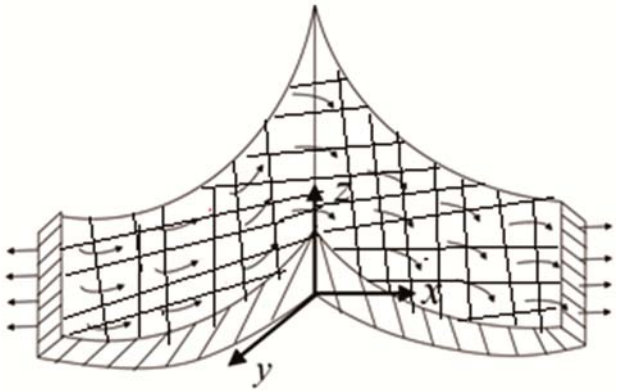

Fig. 1 — Flow geometry of the problem.

$$u\frac{\partial C}{\partial x}+v\frac{\partial C}{\partial y}+w\frac{\partial C}{\partial z}=D_B\frac{\partial^2 C}{\partial z^2}-\Omega\left(C-C_\infty\right) \quad \ldots (5)$$

In the energy Eq. (4), the term $\frac{16\sigma^* T_\infty^3}{3k^*\left(\rho C_P\right)_{nf}}\frac{\partial^2 T}{\partial z^2}$ is obtained by assuming the temperature variation within the flow as small and expanding T^4 in a Taylor series about T_∞ and neglecting higher order terms and using the resulting expression in the Rosseland radiative heat flux[38]: $q_r=-\frac{4\sigma^*}{3k^*}\frac{\partial T^4}{\partial z}$.

The associated boundary conditions for the present problem are:

$$\left.\begin{array}{c} u=U_w=U_0\exp\left[\frac{x+y}{L}\right], v=V_w=V_0\exp\left[\frac{x+y}{L}\right], w=0, \\ -k_f\frac{\partial T}{\partial z}=h_f(T_f-T),\ C=C_w=C_\infty+C_0\exp\left[\frac{B(x+y)}{2L}\right], at\ z=0 \\ u\to 0, v\to 0, T\to T_\infty, C\to C_\infty\ as\ z\to\infty \end{array}\right\} \quad \ldots (6)$$

where u, v and w are velocity components along x, y and z-directions, respectively, υ_f is the kinematic viscosity, T_∞ is the free stream temperature, C_∞ is the free stream nanoparticle concentration, T and C are respectively the temperature and concentration of the fluid, σ is the electrical conductivity of the base fluid, B_0 is the maximum strength of variable magnetic field, ρ_f is the fluid density, U_0, V_0, U_w and V_w are constant velocities, L is the reference length, k_f is the thermal conductivity, h_f is the convective heat transfer coefficient, T_f is the temperature of the fluid heating the surface of the sheet, σ^* is the Stefan-Boltzmann constant, k^* is the mean absorption coefficient of the nanofluid, B is the concentration exponent, Ω is the chemical reaction rate and Ω_0 is a constant. Here ρ_{nf} is the effective density of the nanofluid and $\left(\rho C_p\right)_{nf}$ is the heat capacitance of the nanofluid, defined in literature[13,39,40] as:

$$\left.\begin{array}{c} \rho_{nf}=(1-\phi)\rho_f+\phi\rho_s \\ (\rho C_p)_{nf}=(1-\phi)(\rho C_p)_f+\phi(\rho C_p)_s \end{array}\right\} \quad \ldots (7)$$

where $\left(\rho C_p\right)_f$ and $\left(\rho C_p\right)_s$ are respectively the heat capacitances of base fluid and nanoparticles, ρ_s and ρ_f are the density of pure fluid and nanopartricles respectively.

The effective dynamic viscosity of the nanofluid is described in literature[13,39,40] as:

$$\mu_{nf}=\mu_f\left(1+39.11\phi+533.9\phi^2\right) \quad \ldots (8)$$

where μ_{nf} and μ_f are the effective dynamic viscosities of nanofluid and base fluid, respectively, and ϕ is the solid volume fraction of nanoparticles.

Following the micro-convection model proposed by Patel *et al.*[37], the effective thermal conductivity of nanofluid can be determined as:

$$\left.\begin{array}{c} \frac{k_{nf}}{k_f}=1+\frac{k_s A_s}{k_f A_f}+ck_s P_e\frac{A_s}{k_f A_f} \\ \frac{A_s}{A_f}=\frac{d_f}{d_s}\frac{\phi}{1-\phi} \\ Pe=\frac{u_s d_s}{\alpha_f}, u_s=\frac{2k_B T}{\pi\mu_f d_s^2}, c=25,000 \end{array}\right\} \quad \ldots (9)$$

where k_{nf}, k_f and k_s are respectively the thermal conductivities of nanofluids, base fluids and nanoparticles, A_s and A_f are the heat transfer area corresponding to particles and fluid medium respectively, $c(>0)$ is a constant, Pe is the Peclet number, d_f is the molecular size of the fluid and d_s is the nanoparticle diameter, u_s is the Brownian motion velocity of nanoparticles, α_f is the thermal diffusivity of the fluid, and μ_f is the dynamic viscosity of the fluid.

In order to facilitate the analysis, the boundary layer equations are to be made dimensionless with the help of following similarity transformations:

$$\left.\begin{aligned} u = U_0 \exp\left[\frac{x+y}{L}\right] F'(\eta), v = U_0 \exp\left[\frac{x+y}{L}\right] G'(\eta), \\ w = -\sqrt{\frac{\upsilon_f U_0}{2L}} \exp\left[\frac{x+y}{2L}\right]\left[F(\eta)+\eta F'(\eta)+G(\eta)+\eta G'(\eta)\right], \\ \Theta(\eta) = \frac{T-T_\infty}{T_f-T_\infty}, \Phi(\eta) = \frac{C-C_\infty}{C_w-C_\infty} \\ \eta = \sqrt{\frac{U_0}{2\upsilon_f L}} \exp\left[\frac{x+y}{2L}\right] z \end{aligned}\right\} \quad \ldots (10)$$

Equation (1) is satisfied by the velocity components (u,v,w) indicating that the fluid flow is feasible.

Using Eq. (10), Eqs. (2-6) take the form:

$$\phi_1 F''' + (F+G)F'' - 2(F'+G')F' - \phi_2 PF' = 0 \quad \ldots (11)$$

$$\phi_1 G''' + (F+G)G'' - 2(F'+G')G' - \phi_2 PG' = 0 \quad \ldots (12)$$

$$\frac{1}{\Pr}\left(\phi_3 + \frac{4}{3}\phi_4 Rd\right)\Theta'' + (F+G)\Theta' = 0 \quad \ldots (13)$$

$$\frac{1}{Sc}\Phi'' + (F+G)\Phi' - \left[B(F'+G') + \gamma\right]\Phi = 0 \quad \ldots (14)$$

With reduced boundary conditions:

$$\left.\begin{aligned} F = 0, G = 0, F' = 1, G' = \beta, \Theta'(0) = -B_i\left[1-\Theta(0)\right], \Phi = 1 \text{ at } \eta = 0 \\ F' \to 0, G' \to 0, \Theta \to 0, \Phi \to 0, \quad \text{as} \quad \eta \to \infty \end{aligned}\right\} \quad \ldots (15)$$

where

$$\left.\begin{aligned} P = \frac{2\upsilon_f L}{K_0 U_0}, \beta = \frac{V_0}{U_0}, P_r = \frac{\upsilon_f}{\alpha_f}, R_d = \frac{4\sigma^* T_\infty^3}{k_f k^*}, \\ Bi = \frac{\varepsilon}{k_f\sqrt{\frac{U_0}{2\upsilon_f L}}}, \varepsilon = \frac{h_f}{\exp\left(\frac{x+y}{2L}\right)}, Sc = \frac{\upsilon}{D_B}, \gamma = \frac{2L\Omega_0}{U_0} \end{aligned}\right\} \quad \ldots (16)$$

Here P is the permeability parameter, β is the ratio parameter, P_r is the Prandtl number, R_d is the thermal radiation parameter and Bi is the Biot's number, Sc is the Schmidt number and γ is the chemical reaction parameter. The nanoparticle volume fraction constants $\phi_i (i = 1,2,3,4)$ are defined as:

$$\phi_1 = \frac{\nu_{nf}}{\nu_f} = \frac{1+39.11\phi+533.9\phi^2}{1-\phi+\phi(\rho_s/\rho_f)}, \phi_2 = \frac{\rho_f}{\rho_{nf}} = \frac{1}{1-\phi+\phi(\rho_s/\rho_f)},$$

$$\phi_3 = \frac{1+\frac{k_s}{k_f}\frac{d_f}{d_s}\left(\frac{\phi}{1-\phi}\right)+c\frac{k_s}{k_f}Pe\left(\frac{\phi}{1-\phi}\right)}{1-\phi+\phi[(\rho C_p)_s/(\rho C_p)_f)}, \phi_4 = \frac{1}{1-\phi+\phi[(\rho C_p)_s/(\rho C_p)_f)},$$

The skin friction coefficient along the x- and y-directions can be obtained respectively as:

$$C_{fx} = \frac{\tau_{wx}}{\left(\frac{1}{2}\right)\rho_f U_w^2} = \frac{\mu_{nf}\left(\frac{\partial u}{\partial z}+\frac{\partial w}{\partial x}\right)_{z=0}}{\left(\frac{1}{2}\right)\rho_f U_w^2} \quad \ldots (17)$$

$$C_{fy} = \frac{\tau_{wy}}{\left(\frac{1}{2}\right)\rho_f V_w^2} = \frac{\mu_{nf}\left(\frac{\partial v}{\partial z}+\frac{\partial w}{\partial y}\right)_{z=0}}{\left(\frac{1}{2}\right)\rho_f V_w^2} \quad \ldots (18)$$

where τ_{wx} and τ_{wy} are wall shear stresses.

The dimensionless form of skin friction coefficient along the x- and y- directions are obtained respectively as:

$$\left(\frac{\mathrm{Re}_x}{2}\right)^{\frac{1}{2}} C_{fx} = \left(1+39.11\phi+533.9\phi^2\right)F''(0) \quad \ldots (19)$$

$$\left(\frac{\mathrm{Re}_y}{2}\right)^{\frac{1}{2}} C_{fy} = \left(1+39.11\phi+533.9\phi^2\right)G''(0) \quad \ldots (20)$$

The local Nusselt and Sherwood numbers can be expressed respectively as:

$$Nu_x = \frac{xq_w}{k_f\left(T_f - T_\infty\right)} \quad \ldots (21)$$

$$Sh_x = \frac{xq_m}{D_B\left(C_w - C_\infty\right)} \quad \ldots (22)$$

where q_w and q_m are the wall heat flux and wall mass flux from the stretching surface respectively.

The dimensionless form of local Nusselt and Sherwood numbers are respectively:

$$\left(\frac{\mathrm{Re}_x}{2}\right)^{-1/2} Nu_x = -\frac{x}{L}\left(\frac{k_{nf}}{k_f}+\frac{4}{3}Rd\right)\Theta'(0) \quad \ldots (23)$$

$$\left(\frac{\mathrm{Re}}{2}\right)^{-1/2} Sh_x = -\frac{x}{L}\Phi'(0) \quad \ldots (24)$$

Where $\mathrm{Re}_x = \frac{U_w L}{\upsilon_f}$ and $\mathrm{Re}_y = \frac{V_w L}{\upsilon_f}$ are local Reynolds number.

3 Numerical Technique

The system of coupled and governing Eqs (11–14) together with the suitable boundary conditions given in Eq. (15) are solved using shooting method of the symbolic computer algebra software MATLAB by converting the boundary value problem (BVP) into an initial value problem (IVP) (Seddeek *et al.*[41], Hemalatha[42]). At the initial stage, the highest order term of the differential equation is written in the remaining lower order form as:

$$F''' = \frac{1}{\phi_1}\left[2F'(F'+G') - (F+G)F'' + \phi_2 PF'\right] \quad \ldots (25)$$

$$G''' = \frac{1}{\phi_1}\left[2G'(F'+G') - (F+G)G'' + \phi_2 PG'\right], \quad \ldots (26)$$

$$\Theta'' = -\frac{1}{\Pr\left(\phi_3 + (4/3)\phi_4 Rd\right)}\left[(F+G)\Theta'\right] \quad \ldots (27)$$

$$\Phi'' = Sc\left[-(F+G)\Phi' + \left(B(F'+G') + \gamma\right)\Phi\right] \quad \ldots (28)$$

The aim of the methodology, firstly to reduce the governing equations into a system of first order differential equations and for that, introducing the new variables as:

$$f_1 = F, f_2 = F', f_3 = F'', f_4 = G, f_5 = G', f_6 = G'', f_7 = \Theta, f_8 = \Theta', f_9 = \Phi, f_{10} = \Phi' \quad \ldots (29)$$

Letting $f = \left[F\ F'\ F''\ G\ G'\ G''\ \Theta\ \Theta'\ \Phi\ \Phi'\right]^T$ gives

$$\frac{d}{d\eta}\begin{pmatrix} f_1 \\ f_2 \\ f_3 \\ f_4 \\ f_5 \\ f_6 \\ f_7 \\ f_8 \\ f_9 \\ f_{10} \end{pmatrix} = \begin{pmatrix} f_2 \\ f_3 \\ \frac{1}{\phi_1}\left[2f_2(f_2+f_5) - (f_1+f_4)f_3 + \phi_2 P f_2\right] \\ f_5 \\ f_6 \\ \frac{1}{\phi_1}\left[2f_5(f_2+f_5) - (f_1+f_4)f_{67} + \phi_2 P f_5\right] \\ f_8 \\ -\frac{1}{\Pr\left(\phi_3 + (4/3)\phi_4 Rd\right)}\left[(f_1+f_4)f_8\right] \\ f_{10} \\ Sc\left[-(f_1+f_4)f_{10} + \left(B(f_2+f_5)+\gamma\right)f_9\right] \end{pmatrix} \quad \ldots (30)$$

and the corresponding boundary conditions are written as:

$$\begin{aligned} &f_1(0) = 0,\ f_2(0) = 1, && f_2(\infty) \to 0, \\ &f_4(0) = 0,\ f_5(0) = \beta, && f_5(\infty) \to 0, \\ &f_8(0) = -\mathrm{Bi}\left[1 - f_7(0)\right], && f_7(\infty) \to 0, \\ &f_9(0) = 1, && f_9(\infty) \to 0. \end{aligned} \quad \ldots (31)$$

Secondly, we set this BVP up as an IVP and use an ODE solver in Matlab to numerically integrate this system, with the initial conditions given by:

$$f(0) = \left[0\ 1\ K_1\ 0\ \beta\ K_2\ K_3\ -\mathrm{Bi}\left(1-K_3\right)1\ K_4\right]^T, \quad \ldots (32)$$

Where K_1, K_2 , K_3 and K_4 are unknowns.

Thirdly, guess K_1, K_2 , K_3 and K_4, and solve the Eq. (30) using Matlab's ODE routine. The guess unknown values are which based on the linear interpolation of the boundary value specified on an initial mesh of 10 equally spaced points is made. Continue this process till we reach to the convergence criteria, $|E_i| < tolerance = 10^{-10}$ where the errors are defined as:

$$\begin{aligned} E_1 &= f_2\left(\infty, K_1\right) - F'(\infty), \\ E_2 &= f_5\left(\infty, K_2\right) - G'(\infty), \\ E_3 &= f_7\left(\infty, K_3\right) - \Theta(\infty), \\ E_4 &= f_9\left(\infty, K_4\right) - \Phi(\infty). \end{aligned} \quad \ldots (33)$$

The maximum value of η_∞ representing the ambient conditions was assumed to be 10.

4 Results and Discussion

The investigation of the present study deals with the impact of non-uniform permeability of the medium, variable chemical reaction and thermal radiation on three-dimensional stretched flow of nanofluid. A new micro-convection model known as the Patel model[37] is applied for considerable enhancement of the thermal conductivity and hence, the heat transfer capability of nanofluids. In addition, a convective heat transfer model is employed where the bottom surface of the plate gets heated due to a convection mechanism from a hot fluid of temperature T_f providing a heat

transfer coefficient h_f . The solutions of the transformed governing boundary layer equations along with the modified boundary conditions are achieved through fourth-order Runge-Kutta method. Three different kinds of base fluids such as water, ethylene glycol(30%), ethylene glycol$(50\%)$and three different types of nanoparticles such as Cu (copper), Ag (silver) and Fe_3O_4 (Ferric oxide) have been chosen in the present study. The general and thermal properties of both the base fluids and the nanoparticles are incorporated in Table 1.

The variations of fluid velocity along the axial and transverse directions for different values of permeability parameter *P* are shown in Figs 2 and 3, respectively. In both the directions the deceleration of the fluid motion is attained. The fluid temperature as well as concentration variation for different P values is visualized in Figs 4 and 5, respectively. It is also visualized from these figures that fluid temperature and concentration get enhanced due to rise in values of *P*. The very cause for this result is that porous matrix offers a resistive force that brought about the deceleration of the fluid motion and hence enhances thermal resistance (fluid temperature) and nanoparticle concentration. In fact, had there been no porous matrix, the temperature as well as concentration could not be enhanced in the flow field. An interesting consequence of the temperature as well as concentration profiles due to the presence of porous matrix is that the rise in the fluid temperature and concentration is significant for relatively higher values of the permeability parameter *P*. Such outcomes led to thinner momentum boundary layer and thicker thermal as well as concentration boundary layers.

Figures 6-9 demonstrate the influence of stretching parameter β on axial as well as transverse velocities, temperature and nanoparticle concentration of the fluid. It is observed that axial velocity, temperature and concentration exhibit the same behavior (a decreasing trend) in response to an increase in the stretching ratio parameter β whereas a reverse trend is attained for transverse velocity. The obvious reason for this trend is due to the fact that the stretching ratio is the ratio between the transverse and axial velocities of the stretching sheet. An increase in the stretching ratio means that the transverse velocity becomes larger than the axial velocity. Considering the above concept in mind and focusing on the Figs 6 and 7 it is seen that the axial velocity decreases while the transverse velocity exhibits the opposite trend. It can be

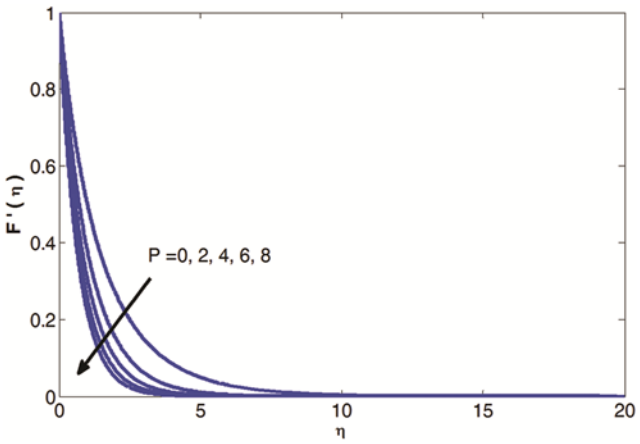

Fig. 2 — Variation of velocity $F'(\eta)$ versus η for different P.

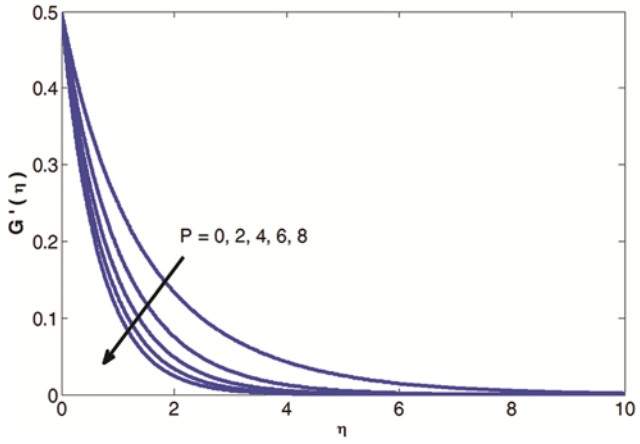

Fig. 3 — Variation of velocity $G'(\eta)$ versus η for different

Table1 — Thermo-physical properties of the base fluid and nanoparticles at *T*=300 K.

	$\rho\ (Kg/m^3)$	$C_P\ (J/KgK)$	$k\ (W/mK)$	$\mu_f\ (Ns/m^2)$	$d_f\ or\ d_s(nm)$
Pure water	997.1	4179	0.613	0.001003	0.24
Ethylene glycol 30%	1034	3736.2	0.489	0.0017613	0.45
Ethylene glycol 50%	1052.1	3301.7	0.432		30-60
Copper (Cu)	8933	385	401		30-60
Silver (Ag)	10500	2235	429		30-60
Ferric oxide (Fe_3O_4)	5180	670	9.7		30-60

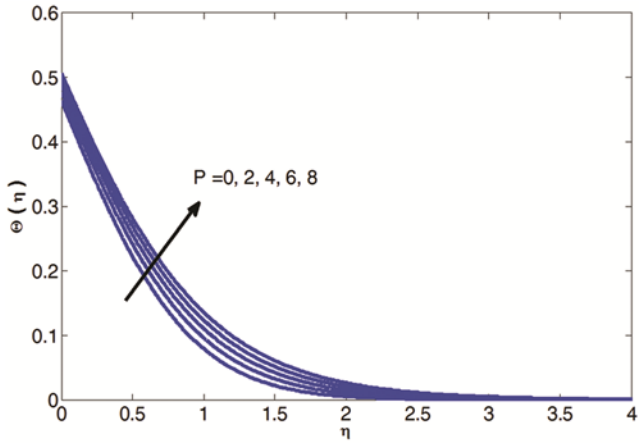

Fig. 4 — Variation of temperature $\Theta(\eta)$ versus η for different P.

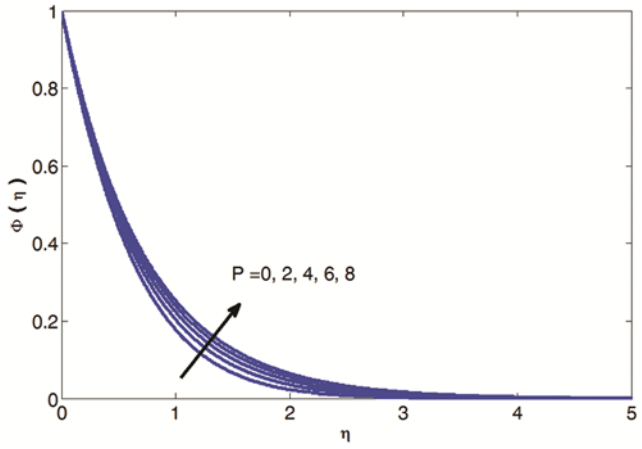

Fig. 5 — Variation of temperature $\Phi(\eta)$ versus η for different P.

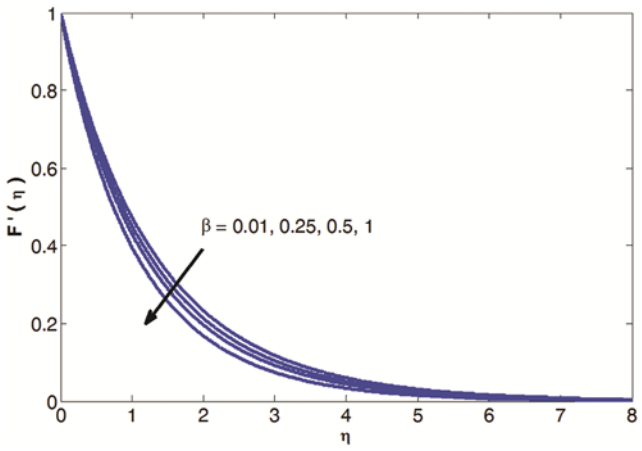

Fig. 6 — Variation of velocity $F'(\eta)$ versus η for different β.

noticed from Figs 8 and 9 that impact of increasing β leads to thinner temperature and concentration boundary layers.

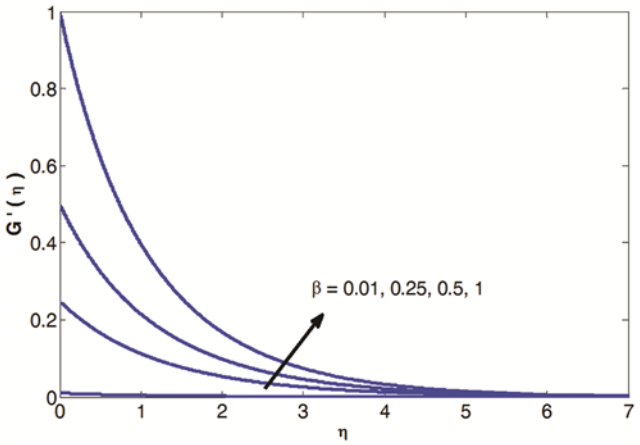

Fig. 7 — Variation of velocity $G'(\eta)$ versus η for different β.

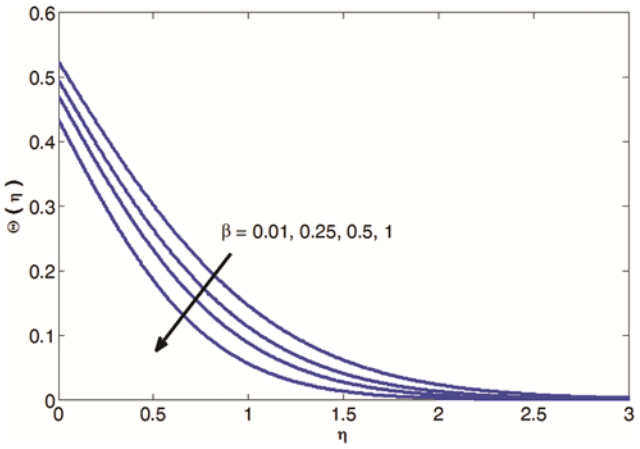

Fig. 8 — Variation of temperature $\Theta(\eta)$ versus η for different β.

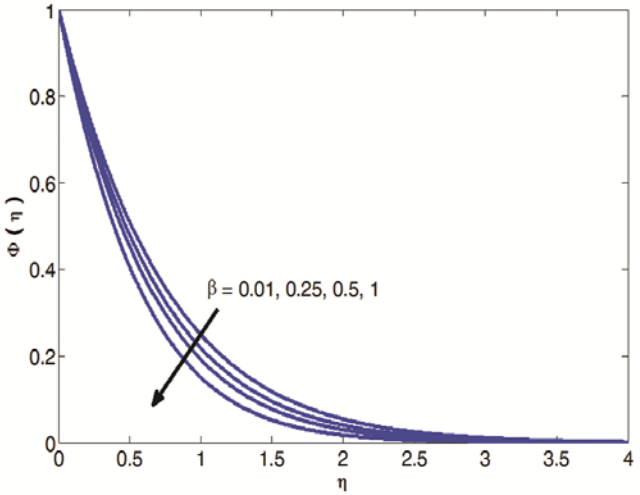

Fig. 9 — Variation of concentration $\Phi(\eta)$ versus η for different β.

Indeed, Prandtl number is the ratio of the kinematic

viscosity to the thermal diffusivity. This influence is revealed by saying that a higher Prandtl fluid such as ethylene glycol (30%) with $\Pr = 13.5$ and ethylene glycol (50%) with *Pr* = 24.4 having a lower thermal diffusivity (lower thermal conductivity) reduces conduction and thereby enhancing variations in thermal characteristics and hence decreasing the thermal resistance (causes a decrease in the fluid temperature) in association with thinner thermal boundary layer whereas the reverse effect is exhibited for a lower Prandtl fluid such as water $(\Pr = 7)$ as shown in Fig. 10. In other words, an increase in the Prandtl number enhances the heat transfer rate at the surface as the wall temperature gradient at the surface gets enhanced.

The behaviour of the thermal radiation on the non-dimensional fluid discloses the outcome that the fluid temperature increases due to an increase in the radiation parameter leading to a significant growth of the thermal boundary layer (Fig. 11). Hence, it is inevitable to maintain the thermal radiation to a minimum so that more heat transfer rate and thereby, more cooling would be accomplished from the stretching surface. It is noticed from Fig. 12 that the non-dimensional temperature and hence, the thermal resistance increases due to an enhancement in the Biot number Bi. However, it is interesting to see from this figure that the increase is significant for higher Bi values. The only reason for this is due to very fact that higher values of Bi brings on stronger convective heating at the sheet leading to more wall temperature gradient which in turn enhances the fluid temperature and thermal boundary layer thickness.

The characteristics of nanoparticle concentration in response to Schmidt number Sc, chemical reaction parameter γ and concentration exponent B are revealed in Figs. 13-15. All indications from these figures confirm that nanoparticle concentration decreases due to increase in Sc, γ and B. Here it is important to note that increase in Sc corresponds to lower molecular diffusivity and shrinking of concentration boundary layer.

Figures 16 and 17 disclose the behavior of the axial as well as the transverse skin friction with the nanoparticle volume fraction for different ratio parameter β. It is well understood from this figure that the axial as well as the transverse skin friction gets reduced due to an increase in the value of β for

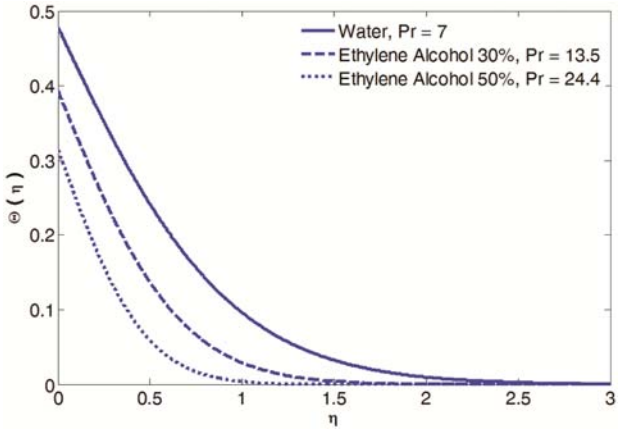

Fig. 10 — Variation of temperature $\theta(\eta)$ versus η for different Pr.

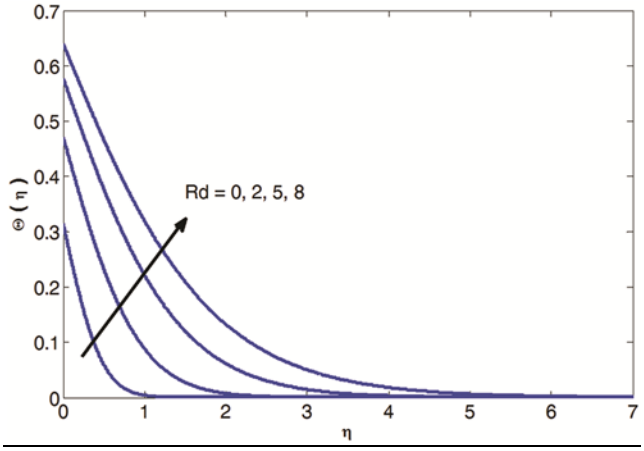

Fig. 11 — Variation of temperature $\theta(\eta)$ versus η for different R_d.

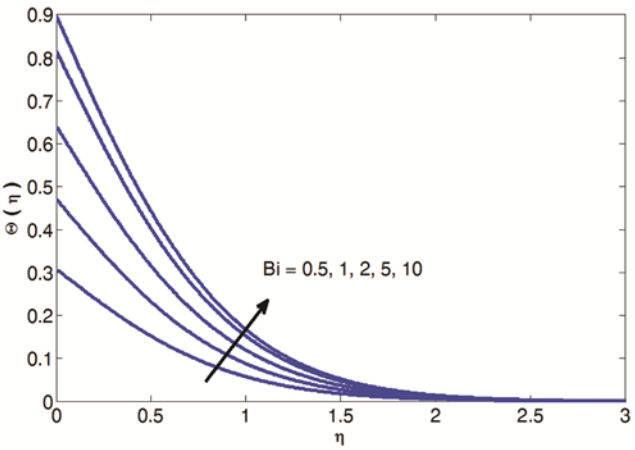

Fig. 12 — Variation of temperature $\theta(\eta)$ versus η for different Bi.

pure water as the base fluid with Cu nanoparticle. In other words, an increase in β brings down in the axial as well as the transverse wall shear stresses in the

entire flow domain. Similar trend is visualized for the behaviour of the axial as well as the transverse skin friction with the nanoparticle volume fraction for different values of permeability parameter P as shown in Figs 18 and 19. Furthermore, the variation of axial as well as the transverse skin friction with the nanoparticle volume fraction decreases in the choice of order of nanoparticles Cu, Ag and Fe_3O_4 as shown in Figs 20 and 21.

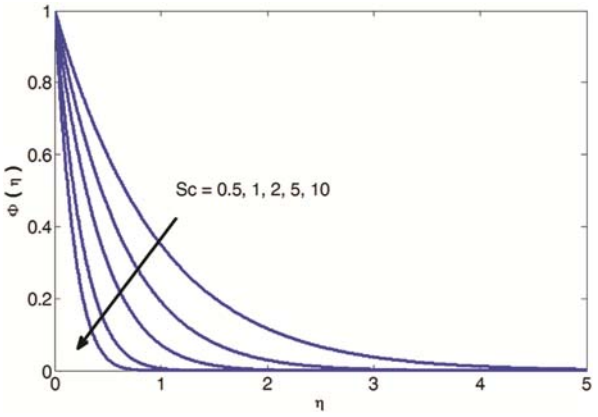

Fig. 13 — Variation of nanoparticle concentration $\Phi(\eta)$ versus η for different Sc .

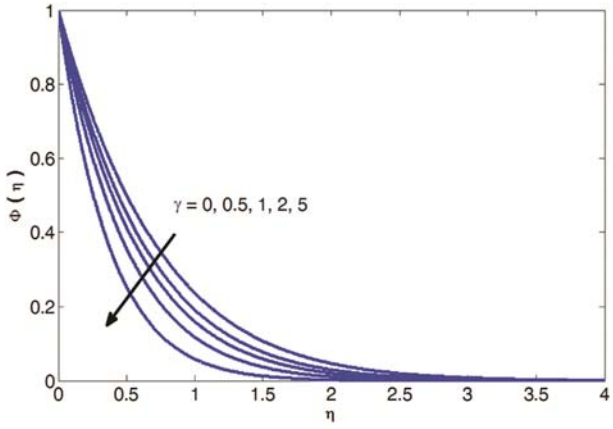

Fig. 14 — Variation of nanoparticle concentration $\Phi(\eta)$ versus η for different γ .

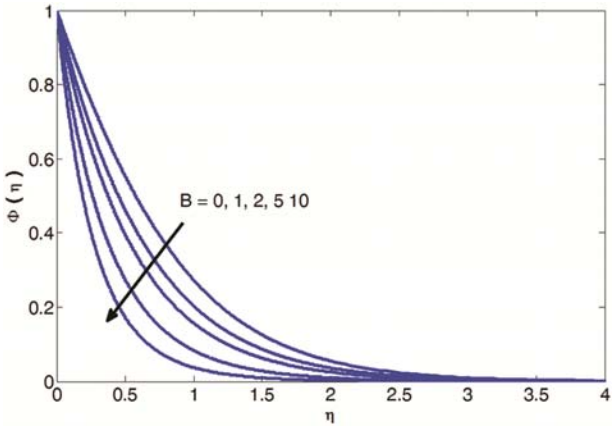

Fig. 15 — Variation of nanoparticle concentration $\Phi(\eta)$ versus η for different B.

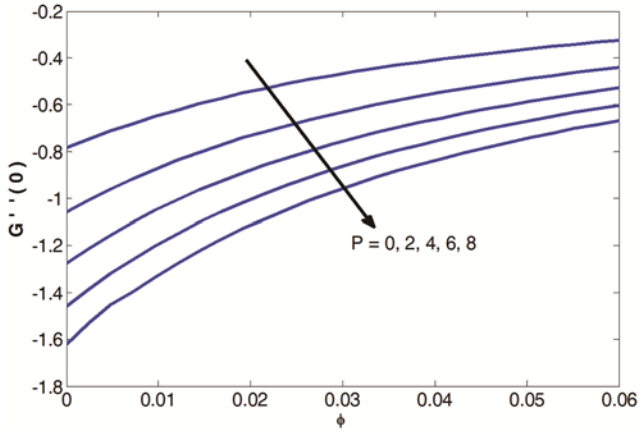

Fig. 19 — Variation of transverse skin friction with φ for different P.

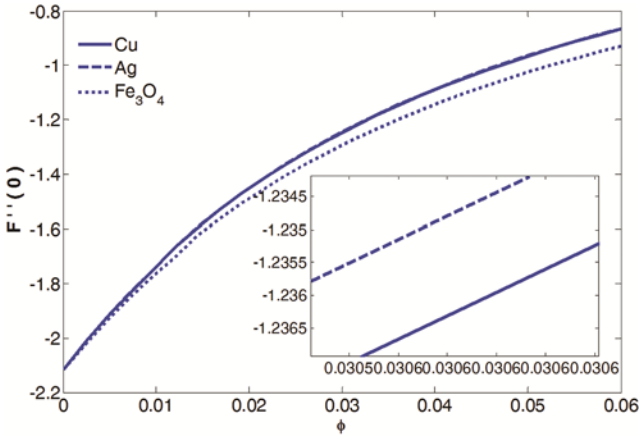

Fig. 20 — Variation of axial skin friction with φ for different nanoparticles.

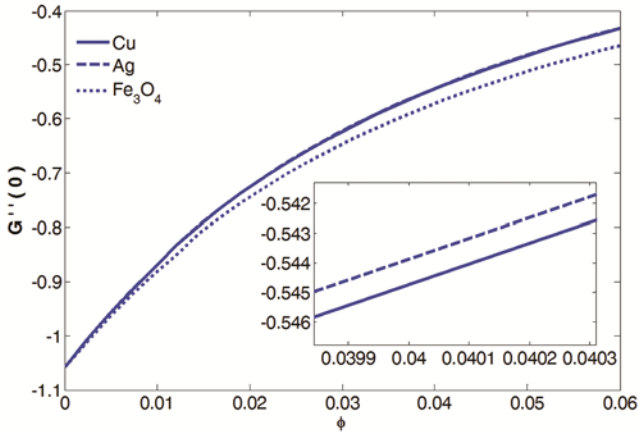

Fig. 21 — Variation of transverse skin friction with φ for different nanoparticles.

The variation of local Nusselt number with the nanoparticle volume fraction ϕ for different values of ratio parameter β and permeability parameter P are seen in Figs 22 and 23, respectively. It is observed

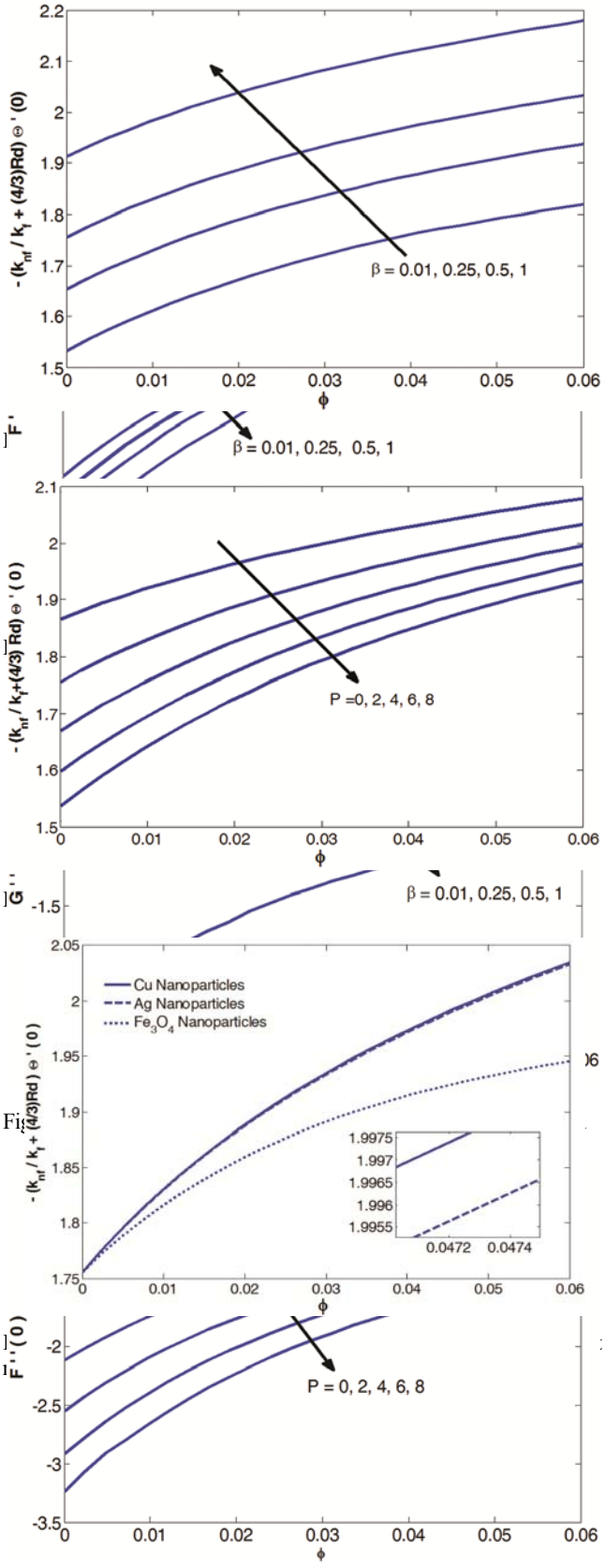

Fig. 18 — Variation of axial skin friction with φ for different P.

that an increase in β decreases the thermal resistance thereby decreasing the fluid temperature which in turn enhances the heat transfer rate from the surface indicating more cooling. On the other hand, increasing values of *P* exhibit the reverse trend for the fluid temperature and hence, the heat transfer rate from the surface. There is a good, valid and compelling reason for such diminution that the resistive force due to porous matrix restrains the fluid motion and boosts the strength of the thermal resistance thereby enhancing the non-dimensional fluid temperature.

Figure 24 shows the decrease of local Nusselt number with ϕ for different nanoparticles in the order of choice viz. Cu, Ag and Fe_3O_4. However, the decrease is significant for the nanoparticle ferric oxide (Fe_3O_4) compared to the other two nanoparticles (Cu and Ag). Figure 25 reveals that the heat transfer rate gets enhanced in association with thermal radiation from lower Prandtl fluid (water with Pr=7) to higher Prandtl fluids (with ethylene glycol 30% having Pr=13.5 and ethylene glycol 50% having Pr=24.4). It may be due to the fact that higher Prandtl fluid corresponds to weaker thermal diffusivity which in turn generates low temperature and hence larger heat transfer rate from the sheet.

The variations of local Sherwood number with ϕ for different values of nanoparticle concentration exponent B and chemical reaction parameter γ are shown in Figs 26 and 27 respectively. It is observed that the mass transfer rate from the surface increases with increase in B and γ .

The results obtained in the present study have been compared and validated with the works of noteworthy researchers viz. Magyari and Keller[43], Liu *et al.*[44] and Nadeem *et al.*[45] as shown in Table 2. The comparison

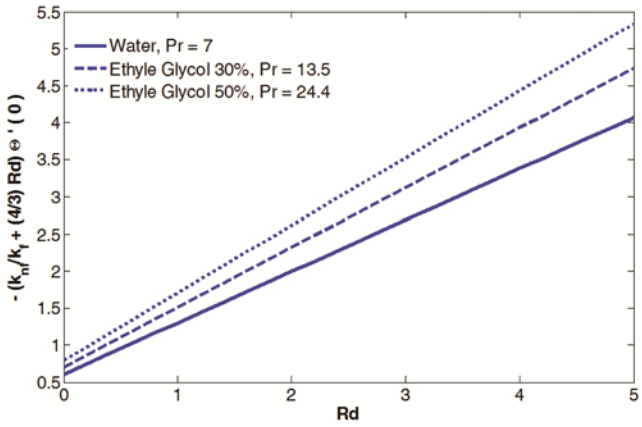

Fig. 25 — Variation of local Nusselt numbers with Rd for different Pr.

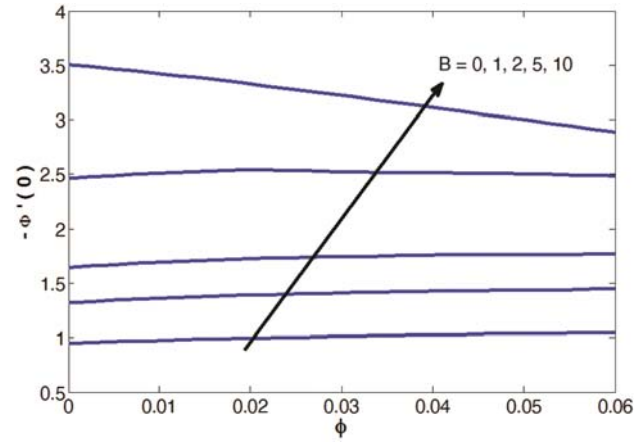

Fig. 26 — Variation of Sherwood number with φ for different B

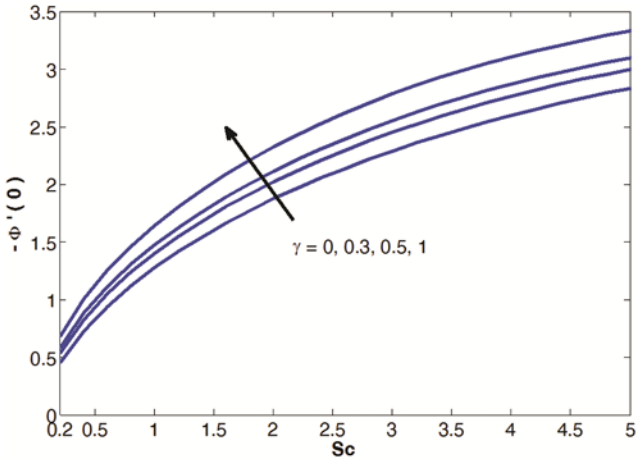

Fig. 27 — Variation of Sherwood number with Sc for different γ.

Table 2 — Comparison with the literature of heat transfer rate for pure fluid M=0, A=0, β =0 results with Magyaari and Keller[43], Liu *et al.*[44], Nadeem *et al.*[45] in the absence of concentration equation.

Pr	Magyaari and Keller[43]	Liu *et al.*[44]	Nadeem *et al.*[45]	Present study
0.7		-0.4258380	-0.42584	-0.42583456
1	-0.549643	-0.54964375	- 0.549646	-0.54964072
5	-1.521243	-1.52123900	-1.521240	-1.52121586
7		-1.8466056	-1.84661	-1.8466092
10	-2.257429	-2.25742372	-2.257424	-2.25737274

Table 3 — Axial and transverse skin friction, local Nusselt number and local Sherwood number with Sc = 1, Rd = 2.

β	P	B	γ	$F''(0)$	$G''(0)$	$-\theta'(0)$	$-\phi'(0)$
0.01	2	1	0.5	-0.91900344	-0.00919003	0.46911927	1.27989984
0.25				-0.96651736	-0.24162934	0.49883800	1.38699844
0.5				-1.01360975	-0.50680487	0.52388398	1.49116055
1				-1.10169753	-1.10169753	0.56250385	1.68154697
0.5	0			-0.74621915	-0.37310958	0.53694668	1.54309079
	4			-1.22263153	-0.61131576	0.51323130	1.45229188
	6			-1.40057273	-0.70028637	0.50388908	1.42063242
	2	0		-1.01360975	-0.50680488	0.52388397	1.04870474
		2		-1.01360975	-0.50680488	0.52388397	1.85904175
		5		-1.01360998	-0.50680499	0.52388363	2.72309268
			0	-1.01360975	-0.50680487	0.52388398	1.28865710
			0.3	-1.01360975	-0.50680487	0.52388398	1.41486126
			1	-1.01360975	-0.50680488	0.52388397	1.66310530

and validation indicate that our result is well-agreed with the results reported earlier[43-45] and have assured the accuracy of our results. In this validation, it is found that an increase in the Prandtl number Pr for a pure fluid decreases the thermal resistance thereby enhancing the heat transfer rate (absolute value).

Table 3 incorporates the variation of local skin friction coefficient, Nusselt number and Sherwood number in response to the parameters β, P, B and γ. It is inferred from the table that increase in β, P and B causes to undermine the axial and transverse skin frictions while it upsurges the heat and mass transfer rates from the sheet.

5 Conclusions

The effects of non-uniform permeability, thermal radiation and variable chemical reaction in three-dimensional flow of nanofluid over a convectively heated stretching sheet have been analyzed. In contrast to previous investigations, non-linear medium permeability, radiative heat flux in the Rosseland approximation and variable chemical reaction are considered. This ensures us that our results are more meaningful and practically viable than the results achieved from previous investigations.The numerical solution of the non-dimensionalized transformed governing equations are obtained. The graphical as well as numerical results is addressed and the essential characteristics of pertinent physical parameters are thoroughly explored.

The major findings of the present study are as follows:

(i) The resistive force offered by the porous matrix has caused the fluid velocity (axial as well as transverse) to decelerate which, in turn, gives upward push to fluid temperature and concentration.

(ii) Axial velocity, fluid temperature and nanoparticle concentration are decreasing functions of ratio parameter β while transverse velocity exhibits opposite behavior in response to β.

(iii) Shrinking of temperature and thermal boundary layer is accounted for enhancement of Prandtl number Pr.

(iv) Fluid temperature is an increasing function of radiation parameter Rd and Biot's number Bi whereas concentration field is a decreasing function of Schmidt number Sc and chemical reaction parameter γ.

(v) The wall shear stresses (axial as well as transverse) follow a descending trend due to increase in the values of permeability parameter P and β in the entire flow domain.

(vi) Axial as well as transverse skin frictions gets reduced for the sequence of nanoparticles Cu, Ag and Fe_3O_4.

(vii) Heat transfer rate gets enhanced due to increase in β whereas reverse trend is visualized in response to increase in P.

(viii) Local Nusselt number gets reduced in the sequence of nanoparticles Cu, Ag and Fe_3O_4 while reverse trend is achieved in sequence of Prandtl fluids such as water (Pr=7), ethylene glycol 30% (Pr=13.5) and ethylene glycol 50% (Pr=24.4).

(ix) The mass transfer rate exhibits the same behavior (increasing trend) in response to ϕ and Sc for different values of B and γ.

References

1 Sakiadis B C, *AIChE J*, 7 (1961) 26.
2 Crane L J, *Z Angew Math Phys*, 21 (1970) 645.
3 Khan S K & Sanjayanand E, *Int J Heat Mass Transf*, 48 (2005) 1534.
4 Hayat T, Imtiaz M & Alsaedi A, *Int J Heat Mass Transf*, 92 (2016) 100.
5 Makinde O D, Khan W A & Khan ZH, *Int J Heat Mass Transf*, 62 (2013) 526.
6 Choi S U S, *ASME Fluids Eng Div*, 231 (1995) 99.
7 Xuan Y & Li Q, *J Heat Transf*, 125 (2003) 151.
8 Khan W & Pop I, *Int J Heat Mass Transf*, 53 (2010) 2477.
9 Nayak M K, *Int J Mech Sci*, 124 (2017) 185.
10 Akber N S, Nadeem S, Haq R Ul & Khan Z H, *Chin J Aeronaut*, 26 (2013) 1389.
11 Makinde O D & Animasaun I L*, Int J Therm Sci*, 109 (2016) 159.
12 Hayat T, Shafique M, Tanveer A & Alsaedi A, *Int J Heat Mass Transf*, 102 (2016) 54.
13 Nayak M K, Akbar N S, Pandey V S, Khan Z H & Tripathi D, *Powder Technol*, 315 (2017) 205.
14 Nayak M K, Akbar N S, Pandey V S, Khan ZH & Tripathi D, *Adv Powder Technol*, 28 (2017) 2159.
15 Nayak M K, Dash G C & Singh L P, *Int J Heat Mass Transf*, 79 (2014) 1087.
16 Bejan A, *Convection heat transfer*, 4th Edn, (Wiley: New York), 2013.
17 Nield I A & Bejan A, *Convection in porous media*, 4th Edn, (Springer: New York), 2012.
18 Malik S & Nayak A K, *Int J Heat Mass Transf*, 111 (2017) 329.
19 Hobold G M, daSilva A K, *Int J Heat Mass Transf*, 108 (2017) 1689.
20 Govender S, *Int J Heat Mass Transf*, 110 (2017) 63.
21 Roy M, Biswal P, Roy S & Basak T, *Int J Heat Mass Transf*, 108 (2017) 468.
22 Makinde O D & Aziz A, *Int J Therm Sci*, 50 (2011) 1326.
23 Mustafa M & Khan J A, *J Mol Liq*, 234 (2017) 287.
24 Makinde O D & Ogulu A, *Chem Eng Commn*, 195 (2008) 1575.
25 Nayak M K, *Meccanica*, 51 (2016) 1699.
26 Daniel Y S & Daniel S K, *Alexandria Eng J*, 54 (2015) 705.
27 Daniel Y S, Aziz Z A, Ismail Z & Salah F, *Chinese J Phys*, 55 (2017) 630.
28 Daniel Y S, Aziz Z A, Ismail Z & Salah F, *J Comput Design Eng*, 5 (2018) 232.
29 Nayak M K, Dash G C & Singh L P, *Arab J Sci Eng*, 40 (2015) 3029.
30 Nayak M K, Shaw S & Chamkha A J, *Thermal Sci Eng Prog*, 5 (2018) 97.
31 Nayak M K, Shaw S, Makinde O D & Chamkha A J, *J Nanofluid*, 7 (2018) 657.
32 Nayak M K, Shaw S & Chamkha A J*, J Nanofluid*, 7 (2018) 646.
33 Mabood F, Shateyi S, Rashidi M M, Momoniat E & Freidoonimehr N, *Adv Powder Technol*, 27 (2016) 742.
34 Mustafa M, Khan J A, Hayat T & Alsaedi A, *Int J Heat Mass Transf*, 108 (2017) 1340.
35 Daniel Y S, Aziz Z A, Ismail Z & Salah F, *Theoretical Appl Mech Lett*, 7 (2017) 235.
36 Nayak M K, Dash G C & Singh L P, *J Appl Anal Comput*, 4 (2014) 367.
37 Patel H E, Sundararajn T, Pradeep T, Dasgupta A, Dasgupta N & Das S K, *Pramana J Phys*, 65 (2005) 863.
38 Brewster M Q, *Thermal radiative transfer properties*, (Wiley: New York), 1972.
39 Pak B C & Cho Y I, *Exp Heat Transf*, 11 (1998) 151.
40 Pourmehran O, Rahimi-Gorji M & Ganji D D, *J Taiwan Inst Chem Eng*, 65 (2016) 162.
41 Seddeek M A, Odda S N, Akl M Y & Abdelmeguid M S, *Comput Mater Sci*, 45 (2009) 423.
42 Hemalatha K, Kameshwaran P K & Madhavi MVDNS, *Sadhana*, 40 (2015) 455.
43 Magyari E & Keller B, *J Phy D Appl Phys*, 32 (1999) 577.
44 Liu C, Wang Hung-H & Peng Yih-F, *Chemical Eng Com*, 200 (2013) 253.
45 Nadeem S, Haq R U l & Khan Z H, *Alex Eng J*, 53 (2014) 219.